Metabolome-Wide Association Study of Primary Open Angle Glaucoma

L. Goodwin Burgess,[1] Karan Uppal,[2] Douglas I. Walker,[2] Rachel M. Roberson,[1] ViLinh Tran,[2] Megan B. Parks,[1] Emily A. Wade,[1] Alexandra T. May,[1] Allison C. Umfress,[1] Kelli L. Jarrell,[1] Brooklyn O. C. Stanley,[1] John Kuchtey,[1] Rachel W. Kuchtey,[1] Dean P. Jones,[2] and Milam A. Brantley Jr[1]

[1]Vanderbilt Eye Institute, Vanderbilt University Medical Center, Nashville, Tennessee, United States
[2]Department of Medicine, Emory University Medical Center, Atlanta, Georgia, United States

Correspondence: Milam A. Brantley Jr, Vanderbilt Eye Institute, Vanderbilt University Medical Center, 2311 Pierce Avenue, Nashville, TN 37232-8808, USA; milam.brantley@vanderbilt.edu.

Submitted: February 17, 2015
Accepted: June 10, 2015

Citation: Burgess LG, Uppal K, Walker DI, et al. Metabolome-wide association study of primary open angle glaucoma. *Invest Ophthalmol Vis Sci*. 2015;56:5020–5028. DOI:10.1167/iovs.15-16702

Purpose. To determine if primary open-angle glaucoma (POAG) patients can be differentiated from controls based on metabolic characteristics.

Methods. We used ultra-high resolution mass spectrometry with C18 liquid chromatography for metabolomic analysis on frozen plasma samples from 72 POAG patients and 72 controls. Metabolome-wide Spearman correlation was performed to select differentially expressed metabolites (DEM) correlated with POAG. We corrected *P* values for multiple testing using Benjamini and Hochberg false discovery rate (FDR). Hierarchical cluster analysis (HCA) was used to depict the relationship between participants and DEM. Differentially expressed metabolites were matched to the METLIN metabolomics database; both DEM and metabolites significantly correlating with DEM were analyzed using MetaboAnalyst to identify metabolic pathways altered in POAG.

Results. Of the 2440 *m/z* (mass/charge) features recovered after filtering, 41 differed between POAG cases and controls at FDR = 0.05. Hierarchical cluster analysis revealed these DEM to associate into eight clusters; three of these clusters contained the majority of the DEM and included palmitoylcarnitine, hydroxyergocalciferol, and high-resolution METLIN matches to sphingolipids, other vitamin D-related metabolites, and terpenes. MetaboAnalyst also indicated likely alteration in steroid biosynthesis pathways.

Conclusions. Global ultrahigh resolution metabolomics emphasized the importance of altered lipid metabolism in POAG. The results suggest specific metabolic processes, such as those involving palmitoylcarnitine, sphingolipids, vitamin D-related compounds, and steroid precursors, may contribute to POAG status and merit more detailed study with targeted methods.

Keywords: glaucoma, metabolomics, plasma, sphingosine, vitamin D, palmitoylcarnitine

Glaucoma is an insidiously progressive optic neuropathy that affects nearly 90 million people worldwide, making it a leading cause of irreversible blindness.[1] The high variation of incidence among races[2] and the variation in clinical manifestations of glaucoma[3] emphasize the need to understand how specific genetic and/or metabolic differences among individuals significantly influence disease status. The risk of glaucoma is increased by multiple genetic factors susceptible to the influence of numerous environmental exposures.[4] Mutations in *MYOC*[5] and *OPTN*[6] have been associated with juvenile open angle glaucoma and normal tension glaucoma, respectively, and have also been found in a small percentage of primary open angle glaucoma (POAG) patients. Genome-wide association studies have found links between common genetic variants and POAG, such as *CAV1* and *CAV2*,[7] as well as *TMCO1* and *CDKN2BAS*.[8] However, in total, these genetic variants linked to glaucoma are thought to account for approximately 5% of all POAG and normal tension glaucoma cases.[9] More recent studies have revealed three new loci, *ABCA1*, *AFAP1*, and *GMDS*, to be associated with POAG,[10] but the extent to which these associations involve the general population has yet to be characterized.

The presence of glaucoma has also been associated with metabolic factors, including an increase in plasma markers of oxidative stress, such as malondialdehyde (MDA) and conjugated diene,[11] as well as reduced total antioxidant status (TAS).[12] However, solitary genetic polymorphisms and single protein or metabolic biomarkers have been limited in their predictive capacity. These biomarker studies hint that future predictive measures are possible, but greater discovery of biomarkers associated with glaucoma is necessary to advance knowledge of the disease mechanism at a personalized level.

Ultrahigh resolution metabolic profiling using liquid chromatography-mass spectrometry (LC-MS) provides a practical approach to personalized medicine and has great potential to advance the evaluation of glaucoma risk. The ultrahigh mass resolution and mass accuracy of current Fourier transform mass spectrometers, coupled with advanced adaptive processing algorithms for data extraction, allow the detection and separation of over 10,000 chemicals in plasma. This includes

metabolites from 146 of the 154 pathways in the Kyoto Encyclopedia of Genes and Genomes (KEGG) human metabolic pathways,[13] providing an effective coverage of central metabolic pathways. Importantly, greater than 90% of the KEGG metabolites have distinct elemental composition[13] so that they can be measured based upon the accurate mass and mass resolution without requiring ion dissociation.[14–16]

Metabolomic analysis of serum and plasma has revealed panels of metabolites that distinguish patients with cardiovascular disease,[17] breast cancer,[18,19] Parkinson disease,[20] and diabetes[21] from control patients. This technique is able to differentiate between individuals despite intraindividual variation due to factors such as dietary intake.[14] We have established this metabolomic method as a powerful tool for assessing risk of ocular disease through identifying metabolites that discriminate neovascular AMD patients from controls.[22]

The purpose of this study was 2-fold: first, to determine whether plasma metabolic profiling can detect systemic metabolic differences between POAG patients and controls; and second, to identify metabolites associated with POAG. Metabolic profiles incorporate both individual biomarkers and entire pathways associated with disease, providing a better understanding of POAG pathophysiology.

Methods

Ethics Statement

This case control study was approved by the Vanderbilt University Human Research Protection Program. Research adhered to the tenets of the Declaration of Helsinki and was conducted in accordance with Health Insurance Portability and Accountability Act regulations. Written informed consent was obtained from all participants prior to study enrollment.

Study Participants

A total of 144 individuals were recruited from the Glaucoma Service at the Vanderbilt Eye Institute (VEI). Cases ($n = 72$) were diagnosed with POAG by a fellowship-trained glaucoma specialist (RWK). Diagnosis of POAG was based on optic nerve appearance characteristic of glaucoma, such as progressive cupping, thinning of the neuroretinal rim, notch formation, and disc hemorrhage. All cases had open iridocorneal angles as determined by gonioscopy examination. Patients with POAG underwent ancillary tests as indicated by their clinical findings, such as visual field testing (Humphrey visual field analyzer; Carl Zeiss Meditec, Dublin, CA, USA); fundus photography of the optic nerves (Zeiss 450+ fundus camera; Carl Zeiss Meditec); and retinal nerve fiber layer assessment with spectral domain optical coherence tomography (Cirrus OCT; Carl Zeiss Meditec). Although elevated intraocular pressure (IOP) was not included as a diagnostic criterion, IOP and central corneal thickness (CCT) were recorded for all POAG patients. Glaucoma treatment history was documented for cases.

Controls ($n = 72$) had no clinical signs of POAG, as determined by the same glaucoma specialist (RWK) using standardized diagnostic criteria, such as normal optic nerve and normal visual field. Exclusion criteria for cases included current or past retinal disease other than glaucoma, such as myopic retinopathy, diabetic retinopathy, or inherited retinopathy. Patients with optic nerve degeneration not secondary to glaucoma, active uveitis or ocular infection, or any ocular surgery within the 60 days prior to enrollment were also excluded. Smoking history was obtained from all participants; history and treatment of comorbidities were documented from each participant's electronic medical record.

Sample Collection

At the time of study enrollment, blood was drawn from study participants using a 21- or 23-gauge butterfly needle into two 3-mL blood collection tubes, each containing 56 USP U lithium heparin. These tubes were centrifuged for 10 minutes at 4°C to pellet blood cells, and 2 mL supernatant were transferred to 1.5 mL conical tubes in 100 μL aliquots and immediately stored frozen at –80°C. Samples were subsequently shipped on dry ice to Emory University. Samples were not thawed, remained frozen during transit, and were frozen at –80°C at Emory prior to metabolomic analysis.

Metabolomic Analysis

Frozen plasma samples from all participants were thawed and analyzed by LC-MS at Emory University as previously described.[14,15,22,23] For analysis, samples were batch randomized into 20-sample batches, with each batch containing an equal number of cases and controls in random order. Pooled reference plasma was run prior to and after each batch for quality control and quality assurance. Plasma sample aliquots (65 μL) were treated with 130 μL acetonitrile (2:1 vol/vol) containing an internal isotopic standard mix (3.5 μL per sample) as previously described.[15,23] The internal standard mix for quality control (Supplementary Table S1) consisted of 14 stable isotopic chemicals covering a broad range of chemical properties represented in small molecules.[15] Samples were mixed and placed on ice for 30 minutes prior to centrifugation for 10 minutes (16,100*g* at 4°C) to remove protein. The supernatants (10 μL) were loaded onto an autosampler (Accela Open Autosampler; Thermo Fisher Scientific, Inc., San Jose, CA, USA) maintained at 4°C and analyzed in triplicate using a mass spectrometer (Thermo LTQ Velos Orbitrap; Thermo Fisher Scientific, Inc.) and C18 chromatography (2.1 × 10 cm; Higgins Analytical, Inc., Targa, Mountain View, CA, USA). Elution was obtained with a formic acid/acetonitrile gradient at a flow rate of 0.35 mL/min for the initial 6 minutes and 0.5 mL/min for the remaining 4 minutes. The first 2-minute period consisted of a 5% solution A (2% [vol/vol] formic acid in water), 60% water, 35% acetonitrile, followed by a 4-minute linear gradient to a 5% solution A, 0% water, 95% acetonitrile. The final 4-minute period was maintained at 5% solution A, 95% acetonitrile. The mass spectrometer was set to collect from mass/charge ratio (*m/z*) 85 to 2000 over 10 minutes. Electrospray ionization was used in positive mode.[14,15] Optimal operating conditions determined for the mass spectrometer (Thermo Fisher Scientific, Inc.) are listed in Supplementary Table S2.

An adaptive processing software package (apLCMS, in the public domain at http://web1.sph.emory.edu/apLCMS/) designed for use with LC-FTMS data was used for peak extraction and quantification of ion intensities.[24] This software provided *m/z* feature tables containing *m/z* values, retention time, and integrated ion intensity for each *m/z* feature, obtained through five major processing steps: (1) noise filter, (2) peak identification, (3) retention time correction, (4) *m/z* peak alignment across multiple spectra, and (5) reanalysis to capture peaks originally missed because of weak signal relative to the signal to noise filter.[24] We used xMSanalyzer (in the public domain at http://sourceforge.net/projects/xmsanalyzer/) to enhance the feature detection process by performing systematic data re-extraction, statistical filtering, and data merger to enhance quality of data extraction.[25] To ensure quality control, each sample was analyzed in triplicate, and a coefficient of variation (CV) was calculated for each *m/z* feature in each sample. Median CV, percent missing values, and a combined quality score were determined for each *m/z*.

Investigative Ophthalmology & Visual Science

Discriminatory *m/z* features were annotated on a targeted basis using the METLIN (in the public domain at http://metlin.scripps.edu/) and Kyoto Encyclopedia of Genes and Genomes (KEEG; in the public domain at http://www.genome.jp/kegg/)[16,17] databases. The following adducts were used for annotation at ±10 ppm mass tolerance: M+H, M+Na, M+H-2H_2O, M+H-H_2O, and M+2Na-H.

Ion Dissociation Mass Spectroscopy (LC-MS/MS)

Ion dissociation mass spectrometry was carried out for representative DEM within the National Institute of Standards and Technology (NIST) Standard Reference Materials (SRM) 1950. Samples were analyzed using a high-resolution mass spectrometer (Q-Exactive; Thermo Fisher Scientific, Inc.) operated in positive ion mode and standard source conditions utilized for the untargeted metabolic profiling. Analyte separation was accomplished on a C18 column and high performance liquid chromatograph (UltiMate 3000; Thermo Fisher Scientific, Inc.), with gradients optimized to match those used on the Surveyor system interfaced to the Velos Orbitrap HRMS. Prior to analysis, plasma proteins were precipitated using acetonitrile (2:1 vol/vol) and allowed to equilibrate for 30 minutes. Collision-induced ion dissociation was accomplished using high purity N_2 at a normalized collision energy of 35%. Confirmation of the identities was completed by comparing the acquired spectra to online databases (MassBank, METLIN), in-silico fragmentation generators (MetFrag), and structural features.

Data Analysis

Descriptive statistics for demographic and clinical variables were calculated. Comparisons between cases and controls were made using the two-tailed *t* test for continuous data (e.g., age) and the two-tailed Fisher exact test for categorical data (e.g., sex, race, smoking, and comorbidities).

In order to increase confidence for selection of discriminating metabolites, xMSanalyzer[20] was used to filter the data to include only *m/z* features for which at least 70% of either group had values. xMSanalyzer also provided batch normalization using ComBat[26] to control for batch effects. Data then underwent log2 transformation to reduce heteroscedasticity and normalize results. We used 10-fold cross-validation accuracy criteria to minimize false positives and to determine the optimal log2 fold-change threshold for filtering, which was 0.05. To determine differences between cases and controls in the filtered *m/z* features, *P* values from LIMMA-based[27] two-class comparison were adjusted for multiple hypothesis testing using the Benjamini-Hochberg false discovery rate (FDR) correction method.[28] Two-way hierarchical cluster analysis (HCA)[13] was used to visualize the relationship between participants and metabolites found to differentiate POAG patients from controls. Analyses were conducted in R (in the public domain at http://www.r-project.org).

Correlation Analyses

Metabolome-wide Spearman correlation analysis was applied to the significant *m/z* features in order to capture any strongly correlated *m/z* features from the raw data. Associations with absolute Spearman correlation greater than 0.3 and FDR < 0.2 were included in the pathway analysis.

Pathway Analysis

Pathway analysis of metabolic features was completed using MetaboAnalyst (in the public domain at www.metaboanalyst.ca), a tool designed specifically for metabolomics studies. This software uses pathway enrichment analysis and pathway topology analysis to translate metabolic trends into defined pathways relevant to the study at hand. We used KEGG ID compound to cross-reference the KEGG metabolic pathway library.

Table 1. Patient Demographic Data and Comorbidity Status

	POAG	Control	*P* Value
Average age, y	67.8	68.5	0.690
Caucasian, %	88.9	97.2	0.097
Females, %	62.5	56.9	0.610
Current smokers, %	5.6	6.9	0.733
Coronary artery disease, %	9.7	15.3	0.451
Hypertension, %	54.2	55.6	1.000
Hyperlipidemia, %	50.0	59.7	0.315
Diabetes, %	19.4	33.3	0.088
Renal disease, %	0.0	2.8	0.497
Thyroid disease, %	19.4	15.3	0.661

Data Access

Data files relevant to this publication will be made available for nonprofit use by researchers upon request.

Results

Subject Characteristics

The study population consisted of 144 patients, including 72 POAG cases and 72 controls. Comparisons between POAG patients and controls in terms of demographic and environmental data, as well as comorbid medical conditions, are presented in Table 1. The mean age of POAG patients did not significantly differ from that of controls, nor did the percentages of Caucasians, females, or smokers. There was no significant difference between cases and controls regarding coronary artery disease, hypertension, hyperlipidemia, diabetes, renal disease, or thyroid disease (Table 1). Disease-related clinical characteristics of POAG patients are presented in Table 2. General ocular health and characteristics are compared between POAG patients and controls in Supplementary Table S3. A higher percentage of POAG patients had best corrected visual acuity worse than 20/40 ($P = 0.003$). Control patients were less likely to have had cataract surgery ($P = 0.034$), but there was no difference between the groups when considering all types of ocular surgery ($P = 0.352$). Supplementary Table S4 shows comparisons between POAG patients and controls in

Table 2. Clinical Characteristic of POAG Patients ($n = 72$)

Clinical Characteristics	
Mean IOP (eye with higher IOP), mm Hg	16.9
No. of patients with IOP > 21 mm Hg, *n* (%)	10 (13.9)
Mean CCT (eye with higher IOP), μm	542.7
Mean HVF MD (eye with worse MD)	−10.01
Glaucoma treatments	
Glaucoma drops only, *n* (%)	38 (52.7)
Glaucoma laser, *n* (%)	34 (47.2)
Glaucoma surgery, *n* (%)	34 (47.2)

IOP, intraocular pressure; CCT, central corneal thickness; HVF, Humphey visual field; MD, mean deviation.

Investigative Ophthalmology & Visual Science

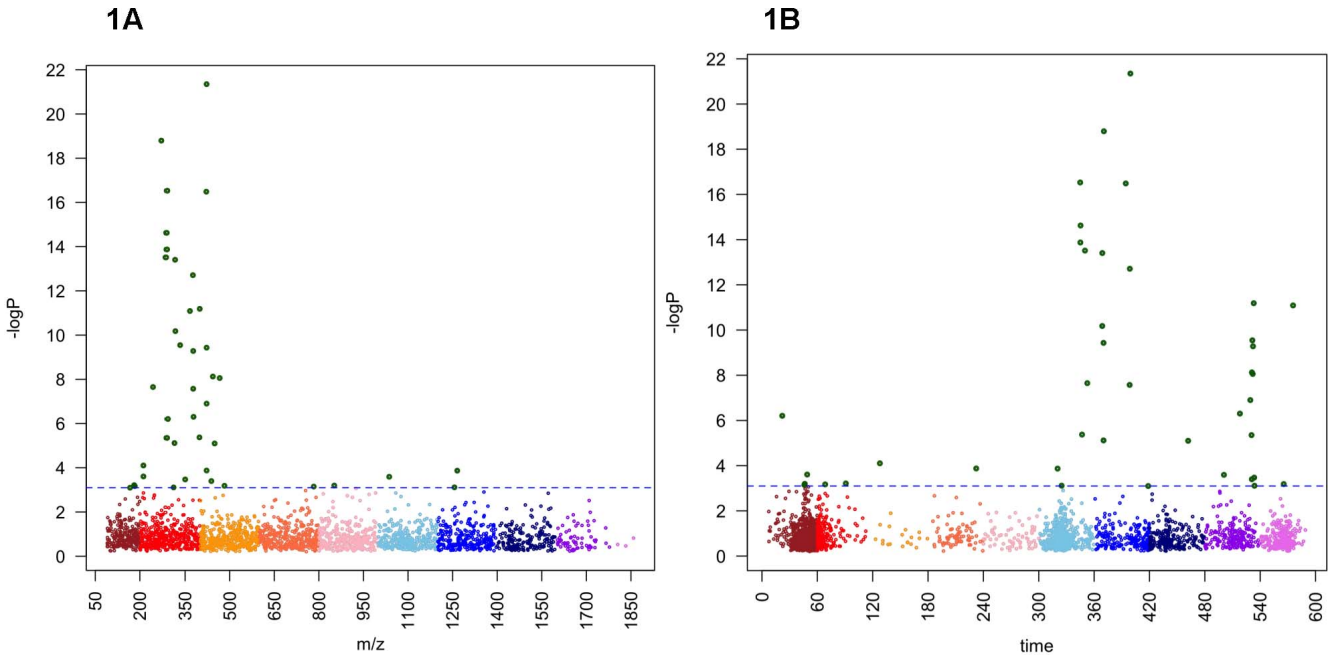

Figure 1. Metabolome-wide association study of POAG. (**A**) Type 1 Manhattan plot of metabolic features of POAG patients ($n = 72$) compared with controls ($n = 72$) shows that 41 of the 2440 *m/z* features differed at FDR = 0.05 (*dotted horizontal line*). Most of these correspond to chemicals with mass less than 500, suggesting that they are relatively small molecules, such as metabolic intermediates, peptides and/or relatively simple lipids. (**B**) Type 2 Manhattan plot shows that the significant features mostly eluted relatively late on the C18 chromatography analysis, indicating that the chemicals are likely to include lipids, such as steroids, terpenoids, fatty acids, and glycerolipids.

terms of systemic medications. There was no difference between the groups in the percentage of patients taking any of nine types of systemic medications.

High-Resolution Metabolomics Data

High-resolution metabolomics uses LC-MS to detect chemicals as ions in the gas phase. The data extraction algorithms are designed to efficiently detect reproducible signals, most of which have not been studied sufficiently to know the identity of the associated chemical. Because of the accurate mass and mass resolution, however, the combination of the *m/z* of an ion and the retention time (RT) from the LC provides a largely unambiguous label even though the chemical identity may be unknown. Mass spectral data from the C18 LC-MS analysis of the 144 samples yielded 19,744 ions (defined by *m/z* and RT), each with associated ion intensity. Given the large number of features, we filtered the data as described in the Methods section to enhance the ability to see the major metabolic differences between POAG patients and controls. After filtering, 2440 *m/z* features were used for statistical analyses.

A metabolome-wide association study (MWAS) of POAG was performed by testing each of the *m/z* features for significant difference between the 72 POAG patients and 72 controls. The results of the analysis are visualized as a Manhattan plot (–log *P* versus *m/z*) in which 41 *m/z* features were significantly different after correction for multiple comparisons at FDR = 0.05 (Fig. 1A; Supplementary Table S5). Assuming that the majority of the differentially expressed metabolites (DEM) were singly charged ions, the *m/z* of most were consistent with being derived from chemicals with mass < 500 Da. Comparison of *m/z* and RT to metabolites previously confirmed by our laboratory showed that the 41 metabolites did not include common metabolic intermediates (e.g., amino acids and metabolites, energy intermediates, nucleotide metabolites, acylcholines) except for palmitoylcarnitine (*m/z* 422.3245, RT 370 seconds). To determine whether the chemicals were hydrophilic or hydrophobic chemicals, data were replotted in a type 2 Manhattan plot (–log *P* versus RT; Fig. 1B). Since the analyses were performed using a reverse phase C18 column, hydrophobic chemicals interact more strongly than hydrophilic chemicals, typically resulting in longer retention time for hydrophobic chemicals. The results showed that most of the significant *m/z* features were chemicals with relatively hydrophobic characteristics, as would be expected from lipids. Because the *m/z* revealed that the chemicals were < 500 Da, the results indicated that the most significant metabolic differences were likely to include relatively simple lipids rather than larger, complex glycosphingolipids.

Two-Way Hierarchical Cluster Analysis

A two-way HCA was performed in order to gain a better understanding of how well the 41 *m/z* features discriminated POAG from controls and to test for similarity of distribution of the features among individuals. The results (Fig. 2) showed separation into two major clusters of individuals, with one consisting of 98% controls (51 individuals designated as group A), and the other consisting of 76% POAG patients (93 individuals designated as group B). As discussed below, group B appeared to have metabolic subgroupings, labeled as B1 ($n = 63$) and B2 ($n = 30$) in Figure 2. All three clusters, A, B1, and B2, became the focus of further analyses.

The 41 *m/z* features grouped into eight major clusters, with four clusters (3, 4, 5, and 7) containing metabolites with higher intensities in POAG patients than in controls and four clusters (1, 2, 6, and 8) containing metabolites with lower intensities in POAG patients (Supplementary Table S6). Combined, clusters 4, 5, and 6 contained the majority of the DEM (30 *m/z* features), demonstrating large groups of associated metabolites (Fig. 2). These results suggest that metabolic pathway and/or

Investigative Ophthalmology & Visual Science

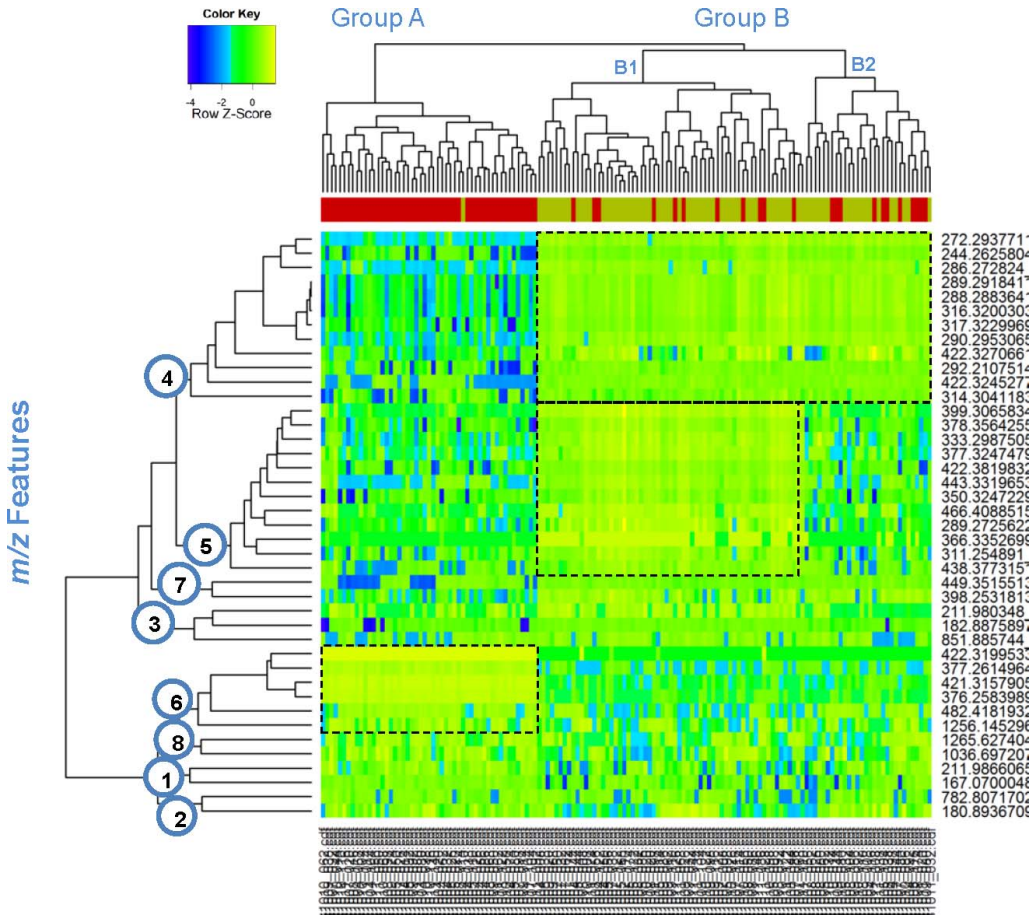

Figure 2. Hierarchical cluster analysis plot of 144 samples versus 41 significant features. The *top border* represents the 144 individuals, with controls as *red* and POAG samples as *green*. The *left border* represents the 41 discriminating metabolites, which formed eight distinct clusters (*blue circles*). Two distinct groups of individuals formed; group A ($n = 51$) consisted of 98% controls, and group B ($n = 93$) consisted of 76% POAG. *Boxes outlined with broken lines* highlight main clusters where metabolites are higher in POAG patients (cluster 4, cluster 5) or higher in controls (cluster 6). These three clusters were subsequently annotated by looking for high-resolution *m/z* matches in the METLIN database. Note that cluster 5 includes metabolites that are higher in only a subset of POAG patients, suggesting a metabolic subtype B1 that differs from metabolic subtype B2 where these metabolites are not elevated.

network differences exist between POAG patients and controls that could provide insight into underlying mechanisms or pathologic responses.

Annotation of Differentially Expressed Metabolites

Cluster 4 contained 12 ions that were higher in POAG than controls; 11 out of 12 eluted with retention times consistent with hydrophobic chemicals, suggesting lipid properties. Two had accurate *m/z* matches (*m/z* 422.3271, 232 seconds; 422.3245, 370 seconds) to palmitoylcarnitine; ion dissociation mass spectroscopy (LC-MS/MS) confirmed that the ion eluting at 370 seconds was indeed palmitoylcarnitine (Supplementary Fig. S1), while the other could be an isobaric species (monoglycerides, triglycerides, or cholane tetrols; Table 3). One group of cluster 4 ions (*m/z* 288.2884, 289.2918, 290.2953, 316.3200, and 317.3230) all putatively matched to sphingoid compounds. The 288.2884 *m/z* matched to C17 sphinganine, and two others (289.2918 and 290.2953) respectively matched the same chemical with one and two ^{13}C atoms (increased by 1.0034). The 316.3200 *m/z* was 28.0316 atomic mass units greater than 288.2884, consistent with being a related lipid differing by two methylene ($-CH_2-$) units (i.e., C19-sphinganine). Additionally, *m/z* 286.2728 matched to both C17 sphingosine and heptadecanedione; although we attempted to obtain MS/MS data to confirm its identity, this feature was present at too low an abundance to obtain useful data. Highly correlated to this feature, *m/z* 244.2626 and *m/z* 272.2938 putatively matched pentadecanone and heptadecanone, respectively. These C15 and C17 chemicals are found in cereal grains. Of the remaining features in cluster 4, *m/z* 314.3041 matched heptadecanediol and *m/z* 292.2108 matched hydroxytetradecanedioic acid.

Cluster 5 contained 12 ions in higher abundance in group B1 than in group A or B2 (Fig. 2). Some of the ions were highly correlated, but there were no obvious multiple forms of single chemicals. The METLIN data included a variety of matches related to vitamin D (Table 3). Four putative matches to fungal sterols (vitamin D2) were present: ergosterol, *m/z* 438.3773, 531 seconds; ergostanol, *m/z* 466.4089, 531 seconds; hydroxyergocalciferol, *m/z* 377.3247, 532 seconds; and dihydroergocalciferol, *m/z* 443.3320, 530 seconds. Ion dissociation (MS/MS) study of *m/z* 377.3247 was consistent with the fragmentation pattern of hydroxyergocalciferol. Putative matches to vitamin D3 metabolites, which are not fungal sterols, were also present in cluster 5, including azacholecalciferol (*m/z* 350.3247, 533 seconds); and fluorohydroxycholecalciferol (*m/z* 399.3066, 533 seconds). These latter two ions

Table 3. Database Matches for Largest Three Clusters of Metabolites

Cluster*	*P* Value	*m/z*	RT, s	Presence in POAG	Match/Comments
4	3.69E-10	422.3245	370	Higher	Palmitoylcarnitine
4	0.000133	422.3271	232	Higher	Monoglyceride (22:5); triglyceride (12:0/18:4/22:6), cholane tetrol
4	2.37E-15	288.2884	345	Higher	C17 sphinganine
4	1.34E-14	289.2918	345	Higher	Probable ^{13}C form of 288.280
4	2.95E-17	290.2953	344	Higher	Probable $^{13}C_2$ form of 288.280
4	6.62E-11	316.3200	368	Higher	Possible 288.2884 plus 2(-CH_2-), C19 sphinganine
4	6.62E-11	317.3230	368	Higher	Probable ^{13}C form of 316.3200
4	3.06E-14	286.2728	350	Higher	C17 sphingosine; heptadecanedione
4	2.23E-08	244.2626	352	Higher	Pentadecanone
4	1.60E-19	272.2938	370	Higher	Heptadecanone
4	7.63E-06	314.3041	370	Higher	Heptadecanediol
4	6.21E-07	292.2108	22	Higher	Hydroxytetradecanedioic acid
5	6.49E-12	399.3066	533	Higher	FluorohydroxyD3; (triterpene); DG(24:0/22:6)
5	4.96E-07	378.3564	518	Higher	No match
5	2.84E-10	333.2988	531	Higher	HODE-cholesteryl ester
5	5.23E-10	377.3247	532	Higher	Hydroxyergocalciferol; DG(24:0/22:6)
5	1.25E-07	422.3820	529	Higher	Diapo-zeta-carotene (terpene)
5	7.48E-09	443.3320	530	Higher	Dihydroergocalciferol; cholestanediol
5	3.37E-04	350.3247	533	Higher	Azacholecalciferol; decaprenol (terpene)
5	8.75E-09	466.4089	531	Higher	Ergostanol
5	4.45E-06	289.2726	531	Higher	No match
5	8.14E-12	366.3353	575	Higher	Heptadecylbenzenediol
5	7.73E-04	311.2549	534	Higher	HODE-methyl ester; monoglyceride
5	3.99E-04	438.3773	531	Higher	Ergosterol
6	3.26E-17	421.3158	394	Lower	Multiple vitamin D analogs; TG (12:0/16:0/20:5)
6	4.48E-22	422.3200	399	Lower	Probable ^{13}C form of 421.3158
6	1.94E-13	376.2584	399	Lower	C19 sphingosine 1-phosphate
6	2.67E-08	377.2615	399	Lower	Probable ^{13}C form of 376.2584
6	0.000255	482.4182	566	Lower	MG(24:1); TG (18:0/18:0/20:0)
6	0.000796	1256.1453	325	Lower	Complex glycosphingolipid

From HCA of features that differed between POAG patients and controls at FDR = 0.05. Searches were conducted at 10 ppm using METLIN. Many features had multiple isobaric matches and representative matches listed will require independent confirmation.

* Clusters are based on HCA as depicted in Figure 2.

also matched terpenes, a large class of compounds that contribute to the syntheses of mitochondrial ubiquinol, cholesterol, steroid hormones, and lipid-soluble vitamins. An additional terpene match (*m/z* 422.3820, 529 seconds) was also present. Among the other matches, *m/z* 366.3353, 575 seconds is noteworthy because it matched heptadecylbenzenediol, a metabolite from cereal grains related to metabolite matches for pentadecanone, heptadecanone, heptadecanedione, and heptadecanediol in cluster 4.

Cluster 6 consisted of six *m/z* features that were quantitatively decreased in POAG relative to controls (Table 3). Two of the features appeared to be ^{13}C forms of others. Assuming that these are ^{13}C forms, three of the features matched triglycerides and two of the features matched C19 sphingosine-1-phosphate.

A small number of matches were present for the other clusters. Of these, cluster 8 contained two features which were decreased in POAG patients and matched MIPC and $M(IP)_2C$, complex sphingolipids. Cluster 7 included a feature (*m/z* 449.3516, 462 seconds) that was higher in POAG patients and matched sphinganine-1-phosphocholine and squalene, a terpene-derived precursor of steroid biosynthesis.[29]

Correlation Among *m/z* Features

Metabolome-wide Spearman correlation analysis was applied to the 41 *m/z* features and produced a correlation network that included the DEM and their top 100 correlated features from the raw data. Like the HCA results, Spearman correlation demonstrated extensive relationships among the 41 *m/z* themselves. Using these data, we examined the relationships of clusters 4, 5, and 6 by selecting representative *m/z* from each and testing for correlations with all other *m/z* features. With a correlation threshold of $|r| > 0.4$ and FDR 0.05, palmitoylcarnitine (422.3245, 370 seconds) and C17-sphingosine/heptadecanedione (*m/z* 286.2728) from cluster 4 were closely associated with C19 sphingosine-1-phosphate from cluster 6 (Fig. 3). All three of these features were associated with hydroergocalciferol (*m/z* 377.3247) and the terpene (*m/z* 422.3820, 529 seconds) from cluster 5. Note that *m/z* 286.2728, which matches both C17-sphingosine and heptadecanedione, was negatively associated with C19-sphingosine-1-phosphate. These results show that the metabolites discriminating POAG from controls are present within a broad network structure involving interacting modules of metabolites.

Pathway Analysis Using MetaboAnalyst

To test whether pathway differences between POAG and controls could be identified with MetaboAnalyst, the broader network structure including the 41 DEMs and their correlated features was used. Three pathways were significant: galactose metabolism, fructose and mannose metabolism, and steroid hormone biosynthesis pathways (Table 4). Significant differences for steroid hormone biosynthesis ($P = 0.00109$) are consistent with the differences observed for terpenes and steroids, many of which are present as multiple isobaric species. MetaboAnalyst uses raw *P* value selection criteria

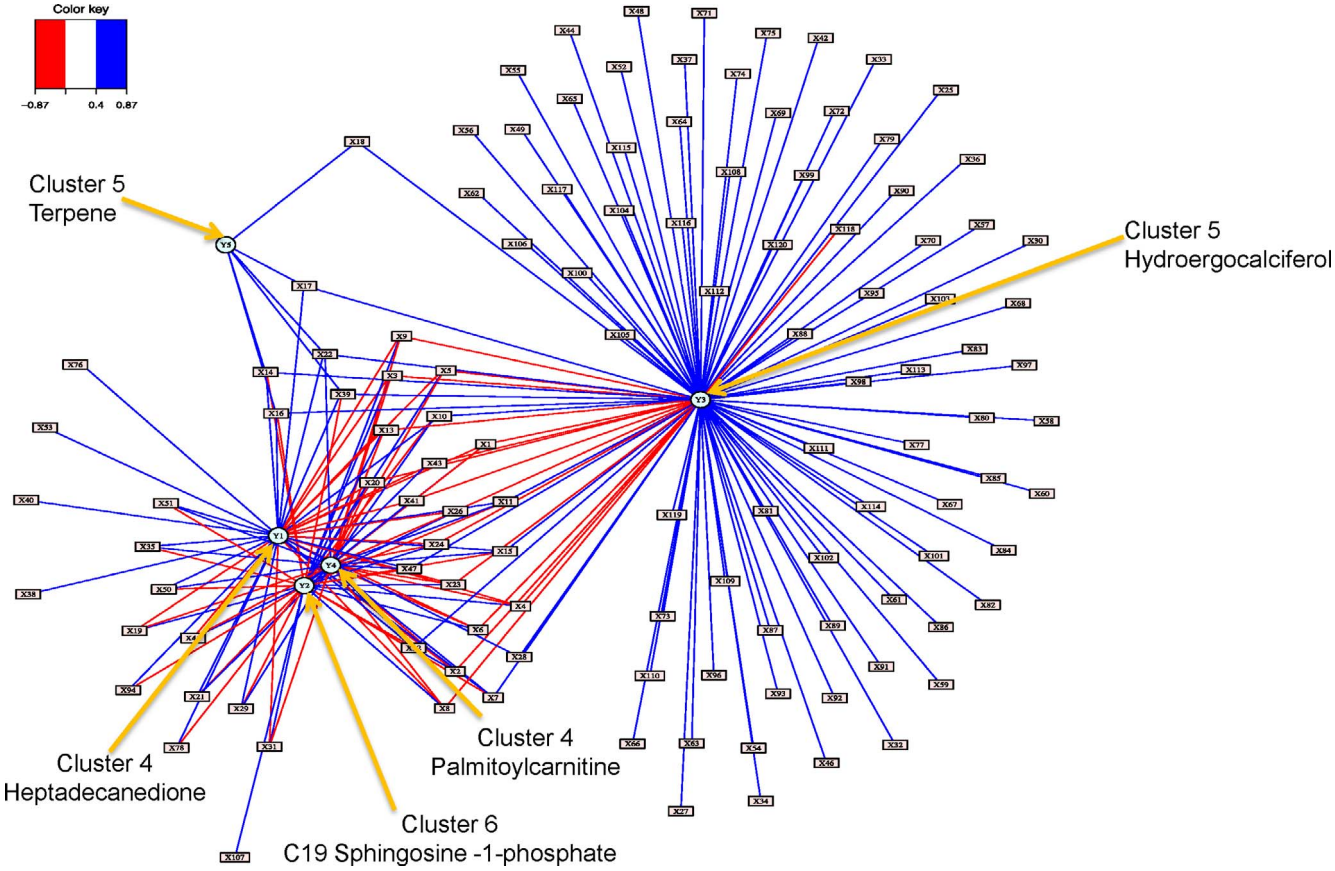

Figure 3. A metabolome-wide association study analysis of five selected *m/z* features (Y1 to Y5) with all other *m/z* features in the feature table. Correlation threshold $|r| > 0.4$ at FDR 0.05.

followed by pathway enrichment analysis to test for pathway significance so that the differences in galactose metabolism ($P = 0.00066$) and fructose and mannose metabolism ($P = 0.0015$) may reflect changes in metabolites that were not significant after false discovery rate correction.

Discussion

This metabolome-wide association study demonstrates the ability to identify systemic alterations in POAG patients that may provide new insight into disease etiology and pathological response. The most apparent trends involve palmitoylcarnitine, sphingolipids, vitamin D-related metabolites, and terpenes. The matches also reveal possible differences in odd-chain fatty acid metabolites and dietary lipids associated with cereal grains. These results support novel hypotheses for future targeted studies investigating causal mechanisms.

Numerous matches indicate changes in fatty acid metabolism in the POAG patients. Palmitoylcarnitine, which functions in the carnitine shuttle system for transport of fatty acids for β-oxidation in the mitochondria, was elevated in POAG cases, consistent with a previous study linking carnitine-palmitoyl transferase II deficiency to normal tension glaucoma.[30] However, other factors can affect mitochondrial palmitoylcarnitine metabolism,[16] suggesting that the increase in palmitoylcarnitine in POAG patients may reflect more generalized impairment of mitochondrial function rather than a specific characteristic of POAG. A previous study has found reduced levels of the omega 3 fatty acids docosahexaenoic (DHA) and eicosapentaenoic acid (EPA) in the blood of POAG patients,[31] the former having even been tested as a treatment option for glaucomatous optic neuropathy.[32] Putative matches to diacylglycerols and triacylglycerols containing DHA and EPA were elevated in POAG cases (Table 3).

Metabolites matching sphingosine and sphinganine were higher in POAG cases than in controls while sphingosine-1-phosphate (S1P) was lower; S1P is a fibrotic mediator[33] and messenger also related to fatty acid metabolism. However, these *m/z* features putatively matched to sphingosine metabolites containing an odd number of carbons in their sphingoid backbones. Sphingosine metabolites in mammals typically contain backbones with an even number of carbons. Never-

Table 4. Metabolic Pathways Found by Metaboanalyst to Associate With POAG Status

Pathway	Total	Expected	Hits	Raw *P*	FDR
Galactose metabolism	41	1.10	6	0.0006577	0.041275
Steroid hormone biosynthesis	99	2.67	9	0.0010985	0.041275
Fructose and mannose metabolism	48	1.29	6	0.0015478	0.041275

Investigative Ophthalmology & Visual Science

theless, odd-numbered carbon chains are found in mammals, thought to be the result of alkylation or branching,[34] and of dietary intake.[35,36] Vitamin B12 finalizes the catabolism of odd-chain fatty acids,[37] and accumulation of odd-chain fatty acid metabolites have also been noted to occur in some mammals due to vitamin B12 deficiency.[38,39] Thus, these results suggest a need for evaluation of multiple mechanisms of fatty acid metabolism in relation to glaucoma status.

A relatively large number of *m/z* putatively matched to vitamin D-related metabolites; 25-Azavitamin D3 is relevant as an inhibitor of the liver 25-hydroxylation of vitamin D3,[40] potentially contributing to deficiency. Vitamin D deficiency is a potential risk factor for open angle glaucoma,[41] and the interrelated metabolites expressed in this study may provide insight into this association. For example, sphingosine kinase (SphK1) is activated by 1α,25-dihydroxyvitamin D3[42]; so inhibition of formation of 1α,25-dihydroxyvitamin D3 can potentially impact conversion of sphingosine to S1P and contribute to the overall metabolic signature of POAG patients. In principle, vitamin D2, a fungal sterol, could also interfere with these mechanisms. Importantly, no significant difference in the percentages of POAG patients and controls taking vitamin D supplements was found in this study ($P = 0.317$), making supplementation an unlikely explanation of the observed differences in vitamin D metabolites. Despite this, the difference between cluster B1 and B2 individuals (Fig. 3) appears to largely be explained by the sterol matches in metabolite cluster 5, suggesting a potential role for this association.

The interactions of these diverse metabolic systems are indicated by correlations of metabolites in Figure 3. The lipids function in energy metabolism and homeostasis, as well as in cell signaling. For instance, vitamin D can control formation of S1P as described above, but S1P has also been shown to function as a messenger to control steroid hormone biosynthesis.[43,44] The detection of differences in metabolites matched to terpenes emphasizes this point. Terpenes are precursors to vitamin D, mitochondrial ubiquinol, cholesterol, and steroid hormones. However, they are also derived from diet so that perturbations could occur from diet or endogenous metabolism. The presence of multiple yeast and fungal sterols further indicates that complex interactions may contribute to POAG. Finally, although no evidence for a causal relationship exists for the multiple cereal lipids that are increased in patients with POAG, the association warrants further investigation because diet or microbiome could impact these levels.

The detection of large numbers of unidentified chemical associated with POAG emphasizes strengths and limitations of this approach. The untargeted metabolomics design allows the evaluation of a wide range of metabolites in POAG patients and does not limit the analysis to a particular type of metabolite or known pathway. At the same time, the use of a single, standardized extraction protocol may have limited the extraction of certain specific metabolites, such as highly nonpolar lipids. Additionally, blood was drawn at patients' regular eye clinic visits, making it likely that metabolites with a wider intraday variation than intersubject variation would not be identified in this study. Our standard sample extraction protocol for untargeted metabolomics is simple and reproducible, and does not call for the addition of antioxidants to plasma prior to storage at −80°C. Thus, some sample oxidation could occur even though samples are never thawed prior to analysis.

This study used high-resolution LC-MS with high mass resolution and mass accuracy, coupled with advanced adaptive processing algorithms for data extraction. Such techniques can accurately identify metabolites within 5 to 10 ppm. However, the putative matches to the metabolomics databases require validation by ion dissociation mass spectrometry (MS/MS). The population size is relatively small and from a limited geographical area, so that further testing in an independent replication cohort is warranted. Initial MS/MS analysis in this study did confirm the identity of two metabolites: palmitoylcarnitine and hydroxyergocalciferol. Finally, although there were no major differences in comorbidities (Table 1) or systemic medications (Supplementary Table S4) between POAG patients and controls, the metabolic changes linked with POAG in this study could be the result of disease or treatment status, and causality cannot be inferred from this association study.

In summary, this MWAS of 72 POAG patients and 72 controls shows that systemic metabolic signatures differentiate cases and controls. The pathway and network analyses show that complex pathway interactions occur and provide a basis to formulate testable hypotheses concerning potential metabolic and dietary factors that could impact disease occurrence and progression. These results indicate that factors impacting mitochondrial metabolism of fatty acids, steroid biosynthesis, and sphingolipid metabolism are worthy of further study. The results also suggest that vitamin D2 and D3 may be mechanistically important. Overall, the results illustrate that metabolomics offers new avenues to explore the pathophysiology of POAG.

Acknowledgments

Supported by National Eye Institute Grants EY022618 (MAB) and EY020894 (RWK); Core Grant P30 EY008126 to Vanderbilt University; an unrestricted grant to Vanderbilt University from Research to Prevent Blindness; and in part by AG038746 (DPJ), ES023485 (DPJ), HL113451 (DPJ), ES019776 (DPJ), OD018006 (DPJ), S10 OD018006 (DPJ), and NIAID contract HHSN272201200031C (DPJ).

Disclosure: **L.G. Burgess**, None; **K. Uppal**, None; **D.I. Walker**, None; **R.M. Roberson**, None; **V. Tran**, None; **M.B. Parks**, None; **E.A. Wade**, None; **A.T. May**, None; **A.C. Umfress**, None; **K.L. Jarrell**, None; **B.O.C. Stanley**, None; **J. Kuchtey**, None; **R.W. Kuchtey**, None; **D.P. Jones**, None; **M.A. Brantley Jr**, None

References

1. Kumar DM, Agarwal N. Oxidative stress in glaucoma: a burden of evidence. *J Glaucoma*. 2007;16:334–343.
2. Friedman DS, O'Colmain BJ, Munoz B, et al. Prevalence of age-related macular degeneration in the United States. *Arch Ophthalmol*. 2004;122:564–572.
3. Moroi SE, Raoof DA, Reed DM, Zollner S, Qin Z, Richards JE. Progress toward personalized medicine for glaucoma. *Expert Rev Ophthalmol*. 2009;4:145–161.
4. Fan BJ, Wang DY, Pasquale LR, Haines JL, Wiggs JL. Genetic variants associated with optic nerve vertical cup-to-disc ratio are risk factors for primary open angle glaucoma in a US Caucasian population. *Invest Ophthalmol Vis Sci*. 2011;52:1788–1792.
5. Stone EM, Fingert JH, Alward WL, et al. Identification of a gene that causes primary open angle glaucoma. *Science*. 1997;275:668–670.
6. Rezaie T, Child A, Hitchings R, et al. Adult-onset primary open-angle glaucoma caused by mutations in optineurin. *Science*. 2002;295:1077–1079.
7. Thorleifsson G, Walters GB, Hewitt AW, et al. Common variants near CAV1 and CAV2 are associated with primary open-angle glaucoma. *Nat Genet*. 2010;42:906–909.
8. Burdon KP, Macgregor S, Hewitt AW, et al. Genome-wide association study identifies susceptibility loci for open angle glaucoma at TMCO1 and CDKN2B-AS1. *Nat Genet*. 2011;43:574–578.

9. Gemenetzi M, Yang Y, Lotery AJ. Current concepts on primary open-angle glaucoma genetics: a contribution to disease pathophysiology and future treatment. *Eye (Lond)*. 2012;26:355–369.
10. Gharahkhani P, Burdon KP, Fogarty R, et al. Common variants near ABCA1, AFAP1 and GMDS confer risk of primary open-angle glaucoma. *Nat Genet*. 2014;46:1120–1125.
11. Chang D, Sha Q, Zhang X, et al. The evaluation of the oxidative stress parameters in patients with primary angle-closure glaucoma. *PLoS One*. 2011;6:e27218.
12. Majsterek I, Malinowska K, Stanczyk M, et al. Evaluation of oxidative stress markers in pathogenesis of primary open-angle glaucoma. *Exp Mol Pathol*. 2011;90:231–237.
13. Jones DP, Park Y, Ziegler TR. Nutritional metabolomics: progress in addressing complexity in diet and health. *Annu Rev Nutr*. 2012;32:183–202.
14. Johnson JM, Yu T, Strobel FH, Jones DP. A practical approach to detect unique metabolic patterns for personalized medicine. *Analyst*. 2010;135:2864–2870.
15. Soltow QA, Strobel FH, Mansfield KG, Wachtman L, Jones DP. High-performance metabolic profiling with dual chromatography-Fourier-transform mass spectrometry (DC-FTMS) for study of the exposome. *Metabolomics*. 2013;9:S132–S143.
16. Go YM, Roede JR, Orr M, Liang Y, Jones DP. Integrated redox proteomics and metabolomics of mitochondria to identify mechanisms of cd toxicity. *Toxicol Sci*. 2014;139:59–73.
17. Dunn WB, Broadhurst DI, Deepak SM, et al. Serum metabolomics reveals many novel metabolic markers of heart failure, including pseudouridine and 2-oxoglutarate. *Metabolomics*. 2007;3:413–426.
18. Asiago VM, Alvarado LZ, Shanaiah N, et al. Early detection of recurrent breast cancer using metabolite profiling. *Cancer Res*. 2010;70:8309–8318.
19. Oakman C, Tenori L, Claudino WM, et al. Identification of a serum-detectable metabolomic fingerprint potentially correlated with the presence of micrometastatic disease in early breast cancer patients at varying risks of disease relapse by traditional prognostic methods. *Ann Oncol*. 2011;22:1295–301.
20. Caudle WM, Bammler TK, Lin Y, Pan S, Zhang J. Using 'omics' to define pathogenesis and biomarkers of Parkinson's disease. *Expert Rev Neurother*. 2010;10:925–942.
21. Wang TJ, Larson MG, Vasan RS, et al. Metabolite profiles and the risk of developing diabetes. *Nat Med*. 2011;17:448–453.
22. Osborn MP, Park Y, Parks MB, et al. Metabolome-wide association study of neovascular age-related macular degeneration. *PLoS One*. 2013;8:e72737.
23. Frediani JK, Jones DP, Tukvadze N, et al. Plasma metabolomics in human pulmonary tuberculosis disease: a pilot study. *PLoS One*. 2014;9:e108854.
24. Yu T, Park Y, Johnson JM. Jones DP. apLCMS–adaptive processing of high-resolution LC/MS data. *Bioinformatics*. 2009;25:1930–196.
25. Uppal K, Soltow QA, Strobel FH, et al. xMSanalyzer: automated pipeline for improved feature detection and downstream analysis of large-scale, non-targeted metabolomics data. *BMC Bioinformatics*. 2013;14:15.
26. Johnson WE, Li C, Rabinovic A. Adjusting batch effects in microarray expression data using empirical Bayes methods. *Biostatistics*. 2007;8:118–1127.
27. Smyth GK. Limma: linear models for microarray data. In: Gentleman R, Carey V, Huber W, Irizarry R, Dudoit S, eds. *Bioinformatics and Computational Biology Solutions Using R and Bioconductor (Statistics for Biology and Health)*. New York: Springer Science+Business Media, Inc.; 2005:397–420.
28. Hochberg Y, Benjamini Y. More powerful procedures for multiple significance testing. *Stat Med*. 1990;9:811–118.
29. Bloch KE. Sterol structure and membrane function. *CRC Crit Rev Biochem*. 1983;14:47–92.
30. Singh R, Dubey R, Montfort J, et al. Carnitine palmitoyl transferase II deficiency: a possible association with progression of normal pressure glaucoma. *Clin Experiment Ophthalmol*. 2012;40:e237–e238.
31. Ren H, Magulike N, Ghebremeskel K, Crawford M. Primary open-angle glaucoma patients have reduced levels of blood docosahexaenoic and eicosapentaenoic acids. *Prostaglandins Leukot Essent Fatty Acids*. 2006;74:157–163.
32. Cellini M, Caramazza N, Mangiafico P, Possati GL, Caramazza R. Fatty acid use in glaucomatous optic neuropathy treatment. *Acta Ophthalmol Scand Suppl*. 1998;41–42.
33. Swaney JS, Moreno KM, Gentile AM, Sabbadini RA, Stoller GL. Sphingosine-1-phosphate (S1P) is a novel fibrotic mediator in the eye. *Exp Eye Res*. 2008;87:367–375.
34. Pruett ST, Bushnev A, Hagedorn K, et al. Biodiversity of sphingoid bases ("sphingosines") and related amino alcohols. *J Lipid Res*. 2008;49:1621–1639.
35. Karlsson AA, Michelsen P, Odham G. Molecular species of sphingomyelin: determination by high-performance liquid chromatography/mass spectrometry with electrospray and high-performance liquid chromatography/tandem mass spectrometry with atmospheric pressure chemical ionization. *J Mass Spectrom*. 1998;33:1192–1198.
36. Merrill AH Jr. Sphingolipid and glycosphingolipid metabolic pathways in the era of sphingolipidomics. *Chem Rev*. 2011;111:6387–6422.
37. Berg JM, Tymoczko JL, Stryer L. *Biochemistry: International Version*. 5th ed. New York: W. H. Freeman; 2002.
38. Kennedy DG, Kennedy S, Blanchflower WJ, et al. Cobalt-vitamin B12 deficiency causes accumulation of odd-numbered, branched-chain fatty acids in the tissues of sheep. *Br J Nutr*. 1994;71:67–76.
39. Akesson B, Fehling C, Jagerstad M. Lipid composition and metabolism in liver and brain of vitamin B12-deficient rat sucklings. *Br J Nutr*. 1979;41:263–274.
40. Onisko BL, Schnoes HK, DeLuca HF. 25-Azavitamin D3, an inhibitor of vitamin D metabolism and action. *J Biol Chem*. 1979;254:3493–346.
41. Yoo TK, Oh E, Hong S. Is vitamin D status associated with open-angle glaucoma? A cross-sectional study from South Korea. *Public Health Nutr*. 2014;17:833–843.
42. Kleuser B, Cuvillier O, Spiegel S. 1Alpha, 25-dihydroxyvitamin D3 inhibits programmed cell death in HL-60 cells by activation of sphingosine kinase. *Cancer Res*. 1998;58:1817–1824.
43. Lucki NC, Sewer MB. Multiple roles for sphingolipids in steroid hormone biosynthesis. *Subcell Biochem*. 2008;49:387–412.
44. Alvarez SE, Milstien S, Spiegel S. Autocrine and paracrine roles of sphingosine-1-phosphate. *Trends Endocrinol Metab*. 2007;18:300–307.